Theory, Synthesis, and Oxygen Reduction Catalysis of Fe-Porphyrin-Like Carbon Nanotube

Duck Hyun Lee,[1] Won Jun Lee,[1] Won Jong Lee,[1] Sang Ouk Kim,[1,*] and Yong-Hyun Kim[2,†]

[1]*Department of Materials Science and Engineering, KAIST, Daejeon 305-701, Republic of Korea*

[2]*Graduate School of Nanoscience and Technology (WCU), KAIST, Daejeon 305-701, Republic of Korea*

(Received 25 August 2010; published 28 April 2011)

We report the synthesis of a Fe-porphyrin-like carbon nanotube from conventional plasma-enhanced chemical vapor deposition. Covalent but seamless incorporation of the 5-6-5-6 porphyrinic Fe-N_4 moiety into the graphene hexagonal side wall was elucidated by x-ray and ultraviolet photoemission spectroscopies and first-principles electronic structure calculations. The resulting biomimetic nanotube exhibits an excellent oxygen reduction catalytic activity with the extreme structural stability over 0.1×10^6 cycles, vastly superior to the commercial Pt-C catalyst.

DOI: 10.1103/PhysRevLett.106.175502 PACS numbers: 61.48.De, 71.15.Nc, 88.30.M−, 88.30.pd

Cathodic oxygen reduction reaction (ORR) is the rate-limiting reaction step for low-temperature fuel cells such as proton-exchange membrane and direct methanol fuel cells. Platinum has been the standard for high activity ORR catalyst for over a century [1–3]. However, the Pt catalyst suffers from the crucial disadvantages of high cost, large overpotential loss, and limited long-term reliability [2,4–6], which have hindered its immediate adoption in the tremendous commercial fuel cell market. Currently, two major approaches are actively pursued to alternate Pt catalyst: Pt alloys [7] and non-Pt catalysts [4–6,8,9]. Pt alloys may pose provisional solutions to reduce Pt consumption, but eventually non-Pt catalysts are demanded.

3*d* transition metal complexes of N_4 macrocycles, for example, Fe-porphyrin and Fe-phthalocyanine, have been investigated as promising non-Pt catalysts [10–12]. It is known that Fe-porphyrin efficiently catalyzes oxygen to water via the so-called ''direct'' four-electron pathway and is generally inert to alcohol oxidation [11]. Nevertheless, Fe-porphyrin-based electrodes have not shown yet any acceptable ORR efficiency. The previous approaches employed simple mixing or delicate attachment of Fe-porphyrin with conductive carbon supports such as carbon black and a carbon nanotube (CNT) and thus resulted in a low density of active catalytic sites and poor electrical and mechanical contacts with such carbon supports [10–12].

In this Letter, we present the theory and synthesis of a Fe-porphyrin-like (Fe-Por) CNT, in which we can directly incorporate many Fe-N_4 moieties into the graphitic side wall [see Fig. 1(a)]. The seamless, covalent incorporation of ''Fe-porphyrin'' into graphene offers not only dense active catalytic sites on surface but also excellent electrical contacts between the catalytic sites and the electron-conducting wires. The novel biomimetic CNT indeed exhibits an excellent ORR catalysis in an electrochemical experiment, outperforming the conventional Pt-C catalyst.

To synthesize a Fe-Por CNT, we prepared highly uniform nanopatterned Fe particles (~ 13 nm diameter, ~36 nm center-to-center distance) on a silicon substrate [13–15]. The plasma-enhanced chemical vapor deposition growth of CNTs from the nanopatterned Fe under an NH_3 environment generated vertical Fe-Por CNT forests with a high yield (~ 40 μm growth in 3 min) [16]. *Ex situ* x-ray photoemission spectroscopy (XPS) analyses have been done for as-grown, air-exposed CNTs with various N-doping levels (0%–8.0%), as shown in Figs. 1(b) and 1(c) for N and Fe, respectively. The N-doping level was readily controlled by the NH_3 partial pressure in the environmental gas, and the maximum doping level of 8.0% was accomplished [14].

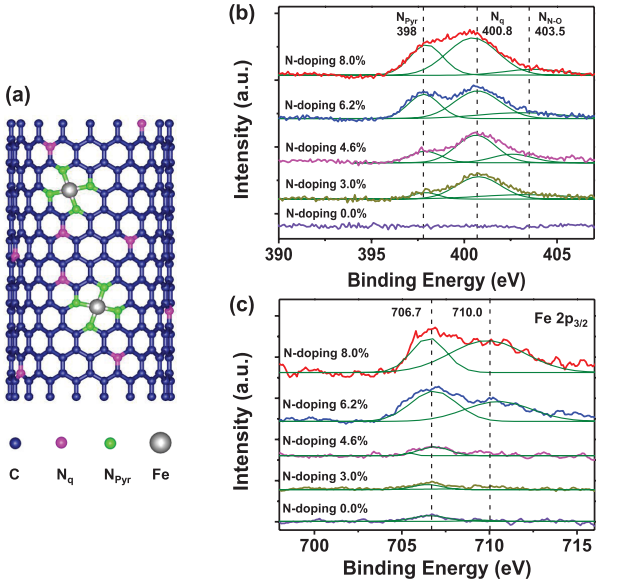

FIG. 1 (color). (a) Schematic illustration of the Fe-Por CNT. The blue, magenta, green, and gray spheres indicate the C, quaternary N (N_q), pyridinic N (N_{Pyr}), and Fe atoms, respectively. XPS spectra of (b) N and (c) Fe for the as-grown CNTs with doping levels of 0.0–8.0%. The N 1*s* peak is deconvoluted into three peaks at 398 (N_{Pyr}), 400.8 (N_q), and 403.5 eV (N_{N-O}). The Fe $2p_{3/2}$ peak is deconvoluted into two major peaks at 706.7 and 710.0 eV.

N XPS peaks are generally classified into four different types, depending on the local chemical environment of N in CNTs: quaternary N (N_q), pyridinic N (N_{Pyr}), pyrrolic N, and nitrogen oxide N ($N_{N\text{-}O}$) [14,17]. Our CNTs showed three peaks for N_{Pyr} (398 eV), N_q (400.8 eV), and $N_{N\text{-}O}$ (403.5 eV) as shown in Fig. 1(b). The absence of pentagonal pyrrolic N is consistent with the fact that our CNTs are free from bamboolike structures in high-resolution TEM images [16]. The Fe XPS peak could be deconvoluted into two major Fe $2p_{3/2}$ peaks at 706.7 and 710.0 eV [17–19]. When the N-doping level was below 4.6%, the N_q peak (400.8 eV) stood out, indicating that quaternary N_q is the dominant defect species, while no appreciable Fe $2p_{3/2}$ peak is observed. However, when the N-doping level exceeded 4.6%, the pyridinic N peak became prominent along with the Fe $2p_{3/2}$ peaks. From the XPS peak area analyses, the ratio of the pyridinic N and the *correlating* Fe $2p_{3/2}$ peaks in the 8.0% N-doped CNT is estimated to 4:1, strongly indicating a formation of porphyrinlike Fe-N_4 complexes. It is also known that the Fe-N_4 moiety could generate two different Fe $2p_{3/2}$ peaks at around 706.7 and 710 eV, depending on its charged state [19]. Because the ratio of N_q and N_{Pyr} is about 3 to 2, the 8.0% N-doped CNT should contain 4.8% quaternary N_q, 3.2% pyridinic N, and 0.8% Fe atoms, as schematically illustrated in Fig. 1(a). Roughly one Fe-N_4 complex per 100 carbon atoms is incorporated in the heavily N-doped CNT.

The formation mechanism of a Fe-porphyrin-like CNT was investigated by first-principles density-functional theory (DFT) calculations [16]. We compared formation energies of various possible substitutional N defects and defect complexes by using the 432-atom (18, 0) CNT model as shown in Fig. 1(a) [16,20]. Pyridinic N should form defect complexes with carbon vacancies in the graphene plane. Three pyridinic N's and a monovacancy could form a triangular defect complex (Pyr-N_3), and four pyridinic N's and a divacancy could form a porphyrinlike rectangular defect complex (Por-N_4) with the 5-6-5-6 pattern [21]. Figure 2(a) shows formation energies of N_q, Pyr-N_3, Por-N_4, and Fe-N_4 as a function of the N chemical potential (μ_N). When μ_N is low, the dominant substitutional defect is N_q, as widely discussed in previous reports [22,23]. When μ_N increases to an N-rich condition, e.g., under elevated NH_3 pressure or increased plasma power, the multi-N defect complex should be stabilized. Many assumed that Pyr-N_3 would be responsible for the pyridinic N in an N-rich environment [22,23]. However, Fig. 2(a) says that Pyr-N_3 is never stabilized in formation energetics with respect to N_q and Por-N_4. Moreover, if bulk Fe is supplied, the Por-N_4 is stabilized further by 2.6 eV with forming Fe-N_4. Recently, it has been suggested that the rectangular pore of Por-N_4 in graphene fits very well for a single Fe atom with the oxidation state of (2 +), resembling the Fe-porphyrin molecule [21]. The crossover from

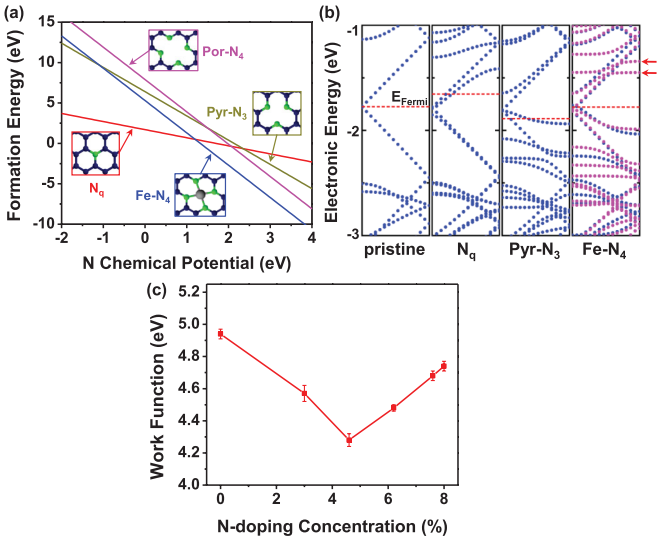

FIG. 2 (color). (a) Calculated formation energies as a function of the N chemical potential μ_N. The insets show the atomic structures of quaternary N_q, Pyr-N_3, Por-N_4, and Fe-N_4. (b) The calculated band structures from Γ to X of the (18, 0) pristine CNT and CNTs incorporated with N_q, Pyr-N_3, and Fe-N_4. For the Fe-N_4-CNT, blue and magenta dots indicate the majority and minority spin states, respectively. In other cases, the spin states were degenerate. The dotted line indicates the Fermi energy (E_F) for each CNT. (c) Work functions of the as-grown CNTs measured by ultraviolet photoemission spectroscopy as a function of the N-doping level.

N_q to Fe-N_4 in Fig. 2(a) well agrees with the XPS trend as the nitrogen doping level increases.

To understand electronic structures of a novel Fe-Por CNT, we performed band structure calculations for the pristine CNT and CNTs incorporated with N_q, Pyr-N_3, and Fe-N_4, as shown in Fig. 2(b). As widely accepted, the N_q defect acts as an electron donor with a raised Fermi energy (E_F) compared to the charge-neutral E_F in the pristine CNT. While the Pyr-N_3 is an electron acceptor with a lowered E_F, the Fe-N_4 is a charge-neutral defect with an almost unchanged E_F. It can be seen that the Fe-Por CNT is still a good electron conductor, although some spin-polarized defect states appear at about 0.3 eV above the E_F.

The Fermi level or work function variations of N-doped CNTs were measured in experiment with ultraviolet photoemission spectroscopy, as shown in Fig. 2(c). The work function curve shows a "V" shape with the minimum at 4.6% N doping. According to the XPS and formation energy analyses, the electron-donating N_q dominates when the N-doping level is below 4.6%. So, the Fermi level is increased, or the work function is decreased. When the N-doping level exceeds 4.6%, however, the charge-neutral Fe-N_4 starts to form. The raised Fermi level by N_q can supply electrons to the otherwise empty defect states of Fe-N_4. Then, the Fermi level is lowered or the

work function is increased. This electron transfer from N_q to Fe^{2+} is responsible for the emergence of the low-energy Fe $2p_{3/2}$ peak at 706.7 eV in heavily N-doped CNTs [19].

Next, the ORR catalysis was characterized for our novel biomimetic electron-conducting CNTs. Three samples were prepared by transferring vertical 10-μm long forests onto a glassy carbon (GC) electrode: a pristine CNT without N doping (CNT|GC), an N_q-dominant CNT with 4.6% N doping (N_q-CNT|GC), and a Fe-porphyrin-like CNT with 8.0% N doping (Fe-Por CNT|GC). Fe particle residues were removed by chemical purification [4,16]. Cyclic voltammograms (CVs) were performed in the N_2- and the O_2-saturated 0.1 M KOH solutions [4,10]. In the N_2-saturated solution, no salient feature was observed for all samples, as shown in Fig. 3(a). The O_2-saturated solution produces an ORR peak at -0.31 V for CNT|GC, -0.26 V for N_q-CNT|GC, and -0.17 V for Fe-Por CNT|GC, respectively. The maximum ORR currents at peaks were 10 (CNT|GC), 40 (N_q-CNT|GC), and 100 μA (Fe-Por CNT|GC). The Fe-porphyrin-like CNT exhibits an outstanding ORR capability, surpassing the performance of the N-only doped CNT [4]. This is consistent with the fact that Fe-N_4 phthalocyanine has ORR activity while H_2-N_4 phthalocyanine without Fe does not [24].

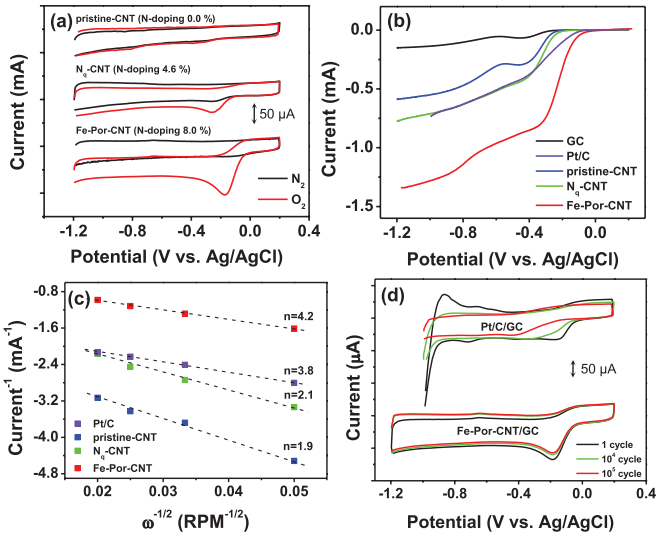

FIG. 3 (color). (a) CVs for the CNT and Fe-Por CNT electrodes with N-doping levels of 0.0% (top), 4.6% (middle), and 8.0% (bottom) in the N_2-saturated (black lines) and the O_2-saturated (red lines) 0.1 M KOH solutions, collected at a scan rate of 25 mV/s. (b) Half-wave RDE voltammograms for ORR at the GC (black), Pt-C|GC (purple), CNT|GC (blue), N_q-CNT|GC (green), and Fe-Por CNT|GC (red) electrodes in O_2-saturated 0.1 M KOH. The scan rate was 5 mV/s, and the electrode rotation rate was 1600 rpm. (c) Koutecky-Levich plots for the Pt-C|GC (purple), N_q-CNT|GC (green), and Fe-Por CNT|GC (red) electrodes with a rotating limiting disk current of -0.5 V vs Ag/AgCl in O_2-saturated 0.1 M KOH. (d) CVs of the Pt-C|GC and Fe-Por CNT|GC electrodes at 1, 10 000, and 100 000 cycles of a continuous potentiodynamic sweep in the O_2-saturated 0.1 M KOH. The scan rate was 100 mV/s.

To reveal detailed microscopic mechanisms of the ORR process, we further performed rotating disk electrode (RDE) voltammograms [16]. Figure 3(b) shows the half-wave steady-state RDE voltammograms for the ORR at bare GC, Pt-C|GC, CNT|GC, N_q-CNT|GC, and Fe-Por CNT|GC in the O_2-saturated 0.1 M KOH. The bare GC electrode was mostly inert. The CNT|GC electrode showed two current drops with onset potentials of -0.26 and -0.61 V. Pt-C/GC and N_q-CNT|GC electrodes exhibited a single current drop at -0.13 and -0.23 V, respectively. These results are all consistent with previous reports [4,10]. Surprisingly, the Fe-Por CNT|GC electrode displayed one giant current drop with the lowest onset potential of -0.10 V. Its steady-state diffusion current at -0.5 V was 3 times larger than that of the pristine CNT and almost twice larger than those of the Pt-C and N_q-CNT. Therefore, the RDE experiment confirmed that the novel biomimetic nanotube is the best ORR catalyst, even better than the commercial Pt-C, in performance.

The ORR pathways could be identified by the Koutecky-Levich plot [Fig. 3(c)] using the RDE data with various rotation rates from 400 to 2500 rpm [10,16]. The ORR proceeds through either (i) a one-step, four-electron process or (ii) a two-step, two-electron process. The former is generally very fast, whereas the latter is rather slow because of relatively stable hydrogen peroxide intermediates [4,10,11]. The determined numbers of transferred electrons per O_2 were 1.9 and 2.1, respectively, for the CNT|GC and N_q-CNT|GC electrodes, representing that the ORR on pristine and N-doped CNTs is the two-step, two-electron process. In contrast, the biomimetic Fe-Por CNT gives 4.2, while Pt-C gives 3.8. The ORR on the novel Fe-Por CNT catalyst is thus the fast four-electron process, as on Pt.

The stability of the Fe-Por CNT electrode was tested by continuous CV measurements between -1.2 and $+0.2$ V. Figure 3(d) shows the CVs of the Pt-C|GC and Fe-Por CNT|GC electrodes after 1, 10 000, and 100 000 cycles of a continuous potentiodynamic sweep in the O_2-saturated 0.1 M KOH at room temperature. In contrast to the serious degradation of catalytic activity of Pt-C, the Fe-Por CNT maintained almost identical voltammetric responses even after 100 000 cycles [25]. The extreme stability can be attributed to the covalent incorporation of Fe-N_4 into the graphene side walls.

The observed fast and stable ORR of Fe-Por CNT is a natural consequence of robust combination of catalytic Fe-N_4 porphyrin with an electron-conducting CNT. As the Fe-N_4 macrocycle does [10], Fe-Por CNT reduces oxygen molecules via the fast one-step process involving four ORR intermediates: $^*O_2$, *OOH, *O, and *OH, where * represents an adsorption site. From our DFT calculations,

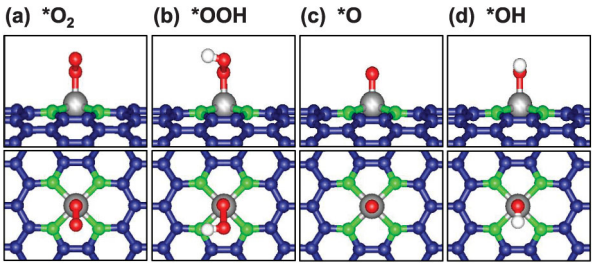

FIG. 4 (color). Side (top) and top (bottom) views of the DFT optimized geometries of (a) $^*O_2$, (b) *OOH, (c) *O, and (d) *OH intermediates on the Fe-N_4 moiety. The blue, green, gray, red, and white spheres represent C, N, Fe, O, and H, respectively.

all the intermediates are stably adsorbed onto the Fe sites as shown in Fig. 4. Particularly, a free O_2 can be adsorbed onto the Fe site with an adsorption energy of 1 eV to form $^*O_2$ [see Fig. 4(a)], which is the most important catalytic intermediate for the associative ORR mechanism [10,26]. Upon the arrival of one electron and one proton, the $^*O_2$ becomes *OOH with a significant increase in the O-O bond length from 1.293 to 1.475 Å. This should facilitate the O-O bond breakage by lowering the reaction energy barrier. As Norskov *et al*. calculated the ORR energetics on Pt(111) under external potential U [26], we also calculated DFT energetics of each ORR step on the Fe-Por CNT, as both listed in Table I. While the associative process on Pt(111) is hindered by a thermodynamic energy barrier of 0.7 eV when $U = 0$, the same on the Fe-Por CNT is a complete downhill. Note that the dissociative mechanism on Pt(111) also goes downhill at $U = 0$ and low oxygen coverage [26].

In conclusion, an excellent ORR catalyst is presented, namely, biomimetic Fe-porphyrin-like carbon nanotubes. This non-Pt catalyst would directly impact on proton-exchange membrane and direct methanol fuel cell technologies in terms of performance, material cost, and stability. Furthermore, by taking advantage of functional diversities of metal-porphyrin complexes and carbon nanotubes, metal-porphyrin incorporated carbon nanotubes or graphenes could have significant implications in various emerging nanotechnologies, including sensors, energy storage, solar cells, artificial photosynthesis, and nanobiomedical applications.

TABLE I. DFT energetics of each ORR step for the associative process on Fe-Por CNT and Pt (111) catalysts, following Ref. [26].

	O_2 + $2H_2$	$^*O_2$ + $2H_2$	*OOH + $1.5H_2$	*O + H_2 + H_2O	*OH + $0.5H_2$ + H_2O	$2H_2O$
Fe-Por CNT	5.06	4.00	3.22	1.29	0.25	0
Pt(111)[a]	4.92	5.59	4.65	2.45	1.75	0

[a]Ref. [26].

We thank Se-Hee Lee for helpful discussion. This work was supported by the NRL (R0A-2008-000-20057-0), WCU (R32-2008-000-10051-0), and NRF grant (R11-2008-058-03002-0) programs funded by the Korean government. Y.-H. K. was supported by the WCU (R31-2008-000-10071-0) and Basic Science Research (2010-0006922) programs through the NRF of Korea.

*Corresponding author.
sangouk.kim@kaist.ac.kr
†Corresponding author.
yong.hyun.kim@kaist.ac.kr

[1] S. Basu, *Recent Trends in Fuel Cell Science and Technology* (Springer, New York, 2007).
[2] R. F. Service, Science **296**, 1222 (2002).
[3] S. H. Joo *et al.*, Nature (London) **412**, 169 (2001).
[4] K. Gong *et al.*, Science **323**, 760 (2009).
[5] M. Lefevre *et al.*, Science **324**, 71 (2009).
[6] B. Winther-Jensen *et al.*, Science **321**, 671 (2008).
[7] J. Fournier *et al.*, J. Electrochem. Soc. **144**, 145 (1997).
[8] J. P. Collman *et al.*, Science **315**, 1565 (2007).
[9] J. Yang *et al.*, Chem. Commun. (Cambridge) 3 (**2008**) 329.
[10] R. Chen *et al.*, J. Phys. Chem. C **113**, 20 689 (2009).
[11] C. W. B. Bezerra *et al.*, Electrochim. Acta **53**, 4937 (2008).
[12] J. H. Jagan, N_4-*macrocyclic Metal Complexes* (Springer, New York, 2006).
[13] D. H. Lee *et al.*, Adv. Mater. **20**, 2480 (2008).
[14] D. H. Lee, W. J. Lee, and S. O. Kim, Nano Lett. **9**, 1427 (2009).
[15] D. H. Lee *et al.*, Adv. Mater. **22**, 1247 (2010).
[16] See supplemental material at http://link.aps.org/supplemental/10.1103/PhysRevLett.106.175502 for details of plasma-enhanced chemical vapor deposition growth of CNTs, first-principles calculations, and electrochemical analyses including CV and RDE voltammograms. Scanning electron microscopy and TEM images of as-grown CNTs, various CVs, and DFT results for a N_q-doped Fe-Por CNT are presented as supplemental figures.
[17] C. D. Wagner *et al.*, *Handbook of X-ray Photoelectron Spectroscopy*, edited by G. E. Muilenberg (Perkin-Elmer, Eden Prairie, MN, 1979).
[18] M. A. Garcia *et al.*, J. Vac. Sci. Technol. B **25**, 1504 (2007).
[19] Y. Bai *et al.*, J. Phys. Chem. C **112**, 6087 (2008).
[20] S. B. Zhang and J. E. Northrup, Phys. Rev. Lett. **67**, 2339 (1991).
[21] W. I. Choi, S.-H. Jhi, K. Kim, and Y.-H. Kim, Phys. Rev. B **81**, 085441 (2010).
[22] C.-L. Sun *et al.*, J. Am. Chem. Soc. **128**, 8368 (2006).
[23] D. Wei *et al.*, Nano Lett. **9**, 1752 (2009).
[24] Y. Nabae *et al.*, Carbon **48**, 2613 (2010).
[25] Similar excellent oxygen reduction and extreme stability of the Fe-Por CNT in acidic condition have been demonstrated in the O_2-saturated $HClO_4$ solution [16].
[26] J. K. Norskov *et al.*, J. Phys. Chem. B **108**, 17 886 (2004).